New investigation of Micro-fluidized bed: The effect of wall roughness and particle size on hydrodynamics regimes

Zhuojun Jiang, Nouria Fatah

Version of Record: https://www.sciencedirect.com/science/article/pii/S1385894721046519
Manuscript_568a5c1bc3d48957763de3a98227aef0

New investigation of Micro-fluidized bed: the effect of wall roughness and particle size on hydrodynamics regimes

Zhuojun Jiang, Nouria Fatah*

Univ. Lille, CNRS, Centrale Lille Institut, Univ. Artois, UMR 8181 – UCCS – Unité de Catalyse et Chimie du Solide, F-59000 Lille, France

* nouria.fatah@centralelille.fr

Abstract

This study presents a new design for Micro-fluidized beds (MFBs), together with a new approach to their hydrodynamic analysis. Two 4 mm MFB reactors were manufactured from glass and resin (constructed by stereo-lithographic 3D printing), to assess the influence of wall roughness on the hydrodynamic characteristics. The novel 3D printing scheme ensures air tightness and good transparency of the reactor. Four types of glass, SiC, Al_2O_3 and TiO_2, belonging to groups B, A/C and C from Geldart's classification, were used to investigate the influence of particle size on their fluidization behavior in MFBs. Three grades of MFB wall roughness were tested. Mechanical vibration energy was applied to the MFBs to improve the quality of fluidization, and to overcome wall friction and cohesive forces. Their hydrodynamic properties were obtained by analyzing pressure fluctuations in the time and frequency domains. The results show that only an appropriate increase in wall roughness was helpful for the suppression of slugging fluidization. The use of mechanical vibrations was found to promote the attenuation or destruction of plug phenomena, thus improving the quality of fluidization of Group A/C and C particles. The feasibility of fluidizing group A/C and C particles has thus been verified in a 3D printed MFB reactors.

Keywords: Micro-fluidized bed; Hydrodynamics; Wall effect; cohesion; 3D design.

1. Introduction

Micro-fluidized beds (MFBs) with a bed diameter (D_t) of only a few centimeters or even millimeters were first proposed by Potic B et al. [1]. Their outstanding surface area-to-volume ratio allows them to be more efficient, and to achieve greater heat dissipation than traditional fluidized beds (TFBs). MFBs are used in various reactions, including biomass pyrolysis, methanation and oxidative dehydrogenation [2-7]. They suffer however from significant challenges in terms of their design and measurement methodologies. A decrease in the value of D_t also leads to the so-called "wall effect", which significantly influences the hydrodynamic characteristics of the bed [8].

The fluidization behaviors from macro- to micro- including pressure drop (Δp), minimum bubbling and slugging, as well as turbulent fluidization characteristics, resulting from MFBs with a small value of D_t , have previously been studied [9-17]. Firstly, the “overshoot” has consistently been observed in MFBs. This refers to the additional pressure that Δp higher than particles bed weight per cross-sectional area (W/A) precede the minimum fluidization point [9, 15]. This value is defined as $\Delta p/(W/A)$ - *1*. The reason for this behavior is that particles in contact with the wall are subjected to a stronger downward frictional force than that encountered in TFBs. Recently, Han et al. [8] analyzed the experimental Δp data reported in the studies of Liu et al. [9] and McDonough et al. [15], showing that a relationship can be established between overshoot and the bed-to-particle diameter ratio (D_t/d_s), defining the boundary between micro and macro fluidization. It was concluded that when D_t/d_s exceeds 150, overshoot disappears and this can be considered as a boundary criterion for the transition between MFBs and TFBs. In addition, when the particles are fully

fluidized, $\Delta p/(W/A)$ tends to unity. However, two contradictory results have been reported: Quan et al. [16] fluidized Group B particles in a MFB with D_t = 4 mm, and found that the value of $\Delta p/(W/A)$ was smaller than unity. This was attributed to some of the particles close to the wall being re-circulated, which would imply that the mass of these particles was being supported by the wall. Conversely, McDonough et al. [15] fluidized the 93 ± 10 μm silica particles in various pseudo-2D fluidized beds with different dimensions (length × width of cross-section (mm): 3×3, 5×5, 5×15, 5×25, 10×10 and 15×15) and found that $\Delta p/(W/A)$ was greater than unity in the 3×3 and 5×5 beds. Xu et al. [18] modeled the fluidization of Group B particles, in a bed with D_t ranging from 8-16 mm, using the CFD-DEM (Computation Fluid Dynamics coupled with Discrete Element Method) model also found similar trend. They attributed that the wall effect resulted in particles being subjected to higher frictional forces, thus sharing part of the Δp. The higher wall friction also plays two-sides roles during transitions from one regime to the other. Some studies reported that the minimum fluidization, minimum bubbling and slugging fluidization were delayed, which was attributed to partial fluidization caused by the resistance effect of friction on some of the particles [16]. However, the turbulent regime would be advanced, due to the suppression of friction on slugging [15]. Overall, progress has been made in studies of the wall effect, which arise from the influence of smaller values of D_t on hydrodynamic behavior. Wall roughness, which can have a significant influence on hydrodynamic behavior, also merits further study.

In addition, the diameter and density of the particles are essential parameters when determining their hydrodynamic behavior in a fluidized bed. Group C particles, also known as cohesive particles, have diameters typically smaller than 30 μm, [19]. It has been reported that it is generally challenging to fluidize group C particles in

TFBs. Indeed, a decrease in particulate size leads to a decrease in mass, and Van der Waals force interactions thus become greater than the influence of gravity, which leads to the mutual attraction of particles, characterized by cohesion of the particle medium and the formation of agglomerates of uncontrollable size and shape [20]. This behavior complicates their fluidization. When the particles agglomerate, the gas can only pass through cracks in the bed, leading to the emergence of channeling and plug phenomena [21]. In the case of some Group C particles with extremely high cohesive forces, the primary particles form small dynamically stable agglomerates that were successfully fluidized at the minimum fluidization velocity (U_{mf}), which is much higher than that of the primary particles [22].

Currently, various methods have been proposed to improve the poor fluidization of Group C particles in TFBs. One approach is to apply external forces, such as mechanical vibrations [23-26], an acoustic field [27, 28] or an electric field [29], in order to overcome the inter-particle forces and break up the natural agglomerates. In addition, agglomerates could be disintegrated through the introduction of large particles [30]. These techniques could potentially alleviate or eliminate the channeling and plugging phenomena. The use of mechanical vibrations, produced by a vibrator acting on the bed or the distributor, is of considerable interest due to their non-invasive characteristics and straightforward disassembly [31]. In particular, the influence of the vibrator's operating parameters on fluidization quality, such as vibration patterns and intensity (amplitude and frequency) has been widely studied. It has been shown that fluidization is improved when either horizontal or vertical vibrations are applied to TFBs [31, 32]. E Marring et al. [33] fluidized Group C particles in a TFB with D_t = 288 mm, under the influence of vibrational intensities ranging from 0 to 5. It was found that U_{mf} decreased with increasing intensity, and

that more cohesive particles required higher energies to achieve good fluidization quality. Yang et al. [26] fluidized SiO_2, TiO_2, and ZnO (10-30 nm) particles, and found that U_{mf} decreases when vibrations are introduced. Wank et al. [34] fluidized boron nitride particles (5 - 10 μm) assisted by vibrations, and it was found that the size of agglomerates decreased with increasing vibrational intensity. However, Xu et al. [35] fluidized talc (4.1 μm) and $CaCO_3$ (5.5 μm) particles using mechanical vibrations. It was found that the size of the agglomerates first decreased, and then increased, when the vibrational intensity was increased, indicating that the latter could not only disintegrate the agglomerates, but also promote their coalescence. Despite this progress, the hydrodynamics of Group C particles in MFBs has not yet been reported.

In the present study, two different Micro-fluidized bed (MFB) designs with D_t = 4 mm are described. These were manufactured from glass and resin (constructed by stereo-lithographic 3D printing (3D-PR) technique). The wall effect in the MFB, arising from the influence of wall roughness on the fluidizing hydrodynamics of Group B particles (glass beads), was first studied. Subsequently, the fluidization behavior of Group A/C particles (glass beads) and various Group C particles (SiC, Al_2O_3 and TiO_2) were compared in a 3D-printed MFB, enhanced by the use of mechanical vibrations. Meanwhile, the influence of vibrational intensity on the fluidization of Group A/C and C particles was also studied. The fluidization behavior of all the particles was assessed on the basis of statistical analyses and the application of a Fast Fourier Transform (FFT) to the measured pressure fluctuations in the bed.

2. Experimental

2.1 Bed Materials

Group B glass beads (noted as glass1), A/C (noted as glass2) and C particles,

including silicon carbide (SiC), aluminum oxide (Al_2O_3) and titanium dioxide (TiO_2), were used for these experiments. The glass beads and SiC, Al_2O_3 and TiO_2 particles were purchased from the Prolabo, Durmax and Kronos companies, respectively.

2.2 Physical properties of the particles

The particle size distributions (**Fig. 1**) of the five aforementioned sets of particles were measured with a light scattering laser instrument (Malvern, Mastersizer 3000). In the experimental setup, the cohesive particles (SiC, Al_2O_3 and TiO_2) were dispersed in a 5% tetrasodium diphosphate / distilled water solution for improved dispersion and to ensure that primary particles would be measured rather than agglomerates. On the basis of their size distribution, the average particle diameter (d_s) was computed according to the definition of the "volume-surface" diameter or "Sauter diameter" [36] (eq. 1). The uniformity of the size distribution was defined by the index C_u [37] (eq. 2), where $C_u < 2$ indicates that the particle size distribution is uniform, and $C_u > 2$ indicates that the particles have a broad size distribution. The density (ρ_s) of all the particles was measured with a Helium gas Pycnometer (Micromeritics, AccuPyc 1330). The average particle diameter can be expressed as:

$d_s = \sum N_i d_i^3 / \sum N_i d_i^2$ (eq. 1),

where N_i is the number of particles in class i and d_i is the average particle diameter in this class. The index C_u is expressed as:

$C_u = d_{i60} / d_{i10}$ (eq. 2),

where d_{i60} and d_{i10} represent the particle diameters with a cumulative percentage of 60% and 10%, respectively.

The physical properties of the particles are shown in **Tab. 1**. It was found that the glass1, glass2 and SiC particles had a narrow size distribution ($C_u < 2$), whereas the Al_2O_3 and TiO_2 particles had a wider size distribution ($C_u > 2$). Although the particles

were optimally dispersed, the measurements revealed the presence of Al_2O_3 and TiO_2 particle agglomerates, due to the strong cohesion between these particles.

In order to further verify the accuracy of the above results, describing the primary particle diameter distributions, images of the particles that could form agglomerates were also recorded by SEM (JSM-7800F, JEOL Ltd.) and TEM (JEOL-2011F, JEOL Ltd.). As shown in **Fig. 2**, the SEM image of the primary Al_2O_3 (a) and TEM images of the primary TiO_2 (b) are consistent with the results measured by the light scattering laser instrument.

2.3 Flowability testing of particles

The flowability of five batches of particles was evaluated using the Hausner index (*HR*) (eq. 3), which is given by the ratio of measured aerated density (ρ_a) and tapped density (ρ_t) [38]. This test was carried out in a 50 ml cylinder. The cylinder was completely filled with particles, and any excess was scraped off using a blade. The corresponding density was recorded as ρ_a. Then, after tapping the cylinder along its vertical axis until the volume could not be further compacted, a second value of density, ρ_t, was determined. The flowability rank was based on the following criteria: HR <1.2 corresponds to free flow (non-cohesive powders), HR >1.4 corresponds to non-free flow (cohesive powders), while 1.2 < HR <1.4 indicates that the particles have an intermediate level of flowability. The *HR* values and flowability rank of the various tested particles are summarized in **Tab. 1**.

$HR = \rho_t / \rho_a$ (eq. 3),

where ρ_t is the tapped bulk density and ρ_a is the aerated bulk density.

2.4 Experimental apparatus

A schematic diagram of the experimental set-up is shown in **Fig. 3**. It consists of a gas supply device, fluidized beds, and signal acquisition and processing devices. All

experiments were carried out at room temperature and pressure. Compressed dried air was used as the fluidizing gas, and its flow rate was controlled by a set of rotameters.

The hydrodynamics of these MFBs were studied by measuring and analyzing the global pressure fluctuations of the bed. The measurement system includes a differential pressure transducer (KELLER, PD-41X) accurate to ±0.2% (full scale), and a data acquisition unit (NI USB-6221, A/D converter with 16-bit resolution). The output signals from the transducer ranged from 0 to 10 V, corresponding to pressures in the range from 0-3000 Pa. The differential pressure transducer has two channels, one of which was connected to the pressure probe in the bed, with the other being directly exposed to the atmosphere. The resulting signals were transferred to a PC workstation and processed using Graphtec (GL900). Matlab (2019b) software was then used to analyze the pressure signals. In addition, a camera was installed in order to capture the different regimes of fluidization, to gain a better understanding of the particle fluidization behavior in the reactor.

Two different D_t = 4 mm MFB designs were used, of which one was made from glass (**Fig. 3 (a)**), and the others were made using 3D-PR (**Fig. 3 (b)**, **(c)** and **(d)**). Porous sintered plates were used as gas distributors for all of the reactors. The details of the distributors are shown in **Tab. S1 in SM.1** (**SM: Supplementary Materials**). The glass reactor was 450 mm long, and the pressure probe was positioned 1.5 mm above the distributor. The connection between the stainless steel probe and the bed was covered with a metal grid with a pore size of 40 μm, to prevent the particles from escaping. The glass column was labeled as Glass. Two additional, almost identical 3D printed columns were designed using Onshape software (**Fig. 4**). Their columns (A) and (B) have a total length of 230 mm, comprising a 100mm long fluidized segment. A disengagement of diameter 36 mm and length 56 mm was connected through an

inclined wall to the fluidized portion, thus avoiding elutriation of the particles. The gas inlet component and the distributor mount were positioned at the base of the column. The only difference between columns (A) and (B) is the position of the pressure probe, in particular 1.5 mm above the distributor on column (A), and below the distributor on column (B). The probe below the distributor was specially designed for Group C particles with a particle size smaller than 15 µm. The position of the pressure probes was chosen to avoid clogging by very small particles. Four columns with different wall roughness were used, to investigate the impact of wall roughness on the hydrodynamics. One of the columns was made of glass (**Fig. 3 (a)**), whereas the others, columns (A) or (B), whose inner surfaces were polished and smoothed to reduce their wall roughness, are noted as ResinAS and ResinBS (**Fig. 3 (b)** and **(c)**). Column (B), whose inner surface was not post-processed, is noted as ResinBWS (**Fig. 3 (d)**). The wall roughness of the Glass, ResinAS, ResinBS and ResinBWS columns was measured on their inner walls using a Mitutoyo-SJ400 profilometer. The roughness value (R_a) was noted as the arithmetic mean height of the roughness profiles. The details of the 3D printing and post-processing steps are provided in **SM.2**, and the characteristics of the MFBs used in this study are listed in **Tab. 2**.

2.5 Mechanical vibrations

A mechanical vibration-assisted technique was used to improve fluidization inside the reactors. Horizontal mechanical vibrations were provided by an electromagnetic vibrator (EMS 755, TOPAS-GMBH, Germany). The positioning of the vibration device and its fixation to the reactor are shown in **Fig. 5**. The vibrational intensity (Λ) used to describe the energy applied to the bed is given in the following expression [23]:

$$\Lambda = A_v(2\pi f_v)^2 / g \quad \text{(eq. 4)}$$

where A_v is the amplitude of the vibrations (mm) and f_v is the frequency (Hz). In this study, A_v ranged from 0 - 0.09 mm, f_v was set to 100 Hz, and the working value of Λ was set to 0, 1.37, 2.34 and 3.43.

2.6 Experimental procedures and data handling

The acquisition parameters initially assumed for the pressure fluctuation data were those reported by Quan et al. [16]. The optimum sampling frequency (f_s) and sampling period were set to 100Hz and 40.96s, respectively, thus leading to $N = 4096$ (2^{12}) samples. Prior to the MFB fluidization tests, the bed was checked for any leakage, and background pressure fluctuations (PF) were measured in the column, in the absence of particles, over the tested range of gas velocities for the Glass and ResinAS beds. In the case of the ResinBS and ResinBWS reactors, due to the differing position of their probes, the background PF produced by the distributor was also measured. The PFs described in the following sections were subtracted from the background values.

For all experiments, the static bed height (H_s) was set to $4D_t$. The experiments were controlled by the rotameters, and the gas velocity was gradually increased from 0 to a maximum value, at which most of the particles had been lifted up to the disengagement segment of the reactor. At this stage, the particles were separated from the fluidization segment, indicating that the fluidization process had been completed. When the fluidization was assisted by mechanical vibrations, the vibrator was first attached at the specified location (**Fig. 5**), and then switched on as described above, in order to acquire the PF data under different vibrational conditions.

At every gas velocity, the PF were recorded after the pressure fluctuations had stabilized. All PF data was collected and processed using statistical analysis and a Fast Fourier Transform (FFT). The mean value ($\bar{x}$), standard deviation (σ), power

spectral density function (PSDF), time–frequency (TF), and dominant frequency (F_d) obtained from the PSDF were analyzed in order to provide a comprehensive description of the fluidization hydrodynamics, together with an improved understanding of various flow patterns such as bubbling, slugging and turbulence. The theory and analysis of all the above parameters can be found in **SM.3** [39, 40].

3. Results and discussion

3.1 Influence of MFB wall roughness on hydrodynamic behavior

Group B particles (glass1) were fluidized in Glass, ResinAS, ResinBS and ResinBWS reactors, in order to study the influence of wall roughness on the MFB hydrodynamics. As shown in **Tab. 2**, the reactors are ranked in order of increasing roughness, R_a, such that Glass (0.23μm) < ResinAS=ResinBS (0.35μm) < ResinBWS (2.09μm). This reveals that, although the stereolithographic technique produced walls with a much higher roughness than in the case of glass components, post-processing of the 3D-printed components (ResinAS and ResinBS) can lead to a wall smoothness close to that observed with glass reactors.

The normalized pressure drop ($\Delta p/(W/A)$) is defined as the ratio of the average pressure fluctuations (Δp) to the particles' bed weight per cross-sectional area (W/A). **Fig. 6 (a)** plots $\Delta p/(W/A)$ as a function of gas velocity (U_g), showing that the overshoot phenomenon which occurs prior to the minimum fluidization point, emerged only in the ResinBWS reactor having the highest wall roughness. This behavior can be explained by the higher surface roughness, which increases the contact area between particles and the wall, thereby exposing the fluidized particles to higher frictional resistance [41]: the mobility of the particles is thus restricted and more energy is needed to fluidize them, which leads to the overshoot shown in **Fig. 6 (a)**. Although overshoot can also occur when D_t becomes very small, as has been

reported in several studies [9, 15], it is shown in the present study that increased wall roughness can also produce the wall effect.

In **Fig. 6 (a)**, it can be seen that with increasing roughness, the normalized pressure drop $\Delta p/(W/A)$ that reached a plateau with increasing U_g, when the particles were fully fluidized (the average value of the plateau over the fluidization zone was noted as $\Delta p/(W/A)_{ff}$), would increase and be higher than unity in the ResinAS, ResinBS, and ResinBWS reactors. The ResinAS and ResinBS reactors were adjusted to understand whether this trend was related to the position of the probe. It was found that $\Delta p/(W/A)_{ff}$ in the ResinBS reactor was slightly higher than in ResinAS, but still smaller than the value measured for the ResinBWS reactor. This implies that the observed changes in $\Delta p/(W/A)_{ff}$ was not related to the different probe positions used in the Resin reactors. Xu et al. [18] observed a similar trend, by simulating the fluidization of Group B particles in an 8 mm bed, with a particle friction coefficient increasing from 0 to 0.4. In parallel, these authors further simulated the forces exerted by the wall on the particles. The results of this study reveal that the overall tangential force was exerted downwards, and increased with increasing particle-wall friction coefficient. This suggests that friction contributed to the pressure drop Δp, thus resulting the value of $\Delta p/(W/A)_{ff}$ was greater than unity.

Fig. 6 (b) plots the standard deviation (σ) of Δp, as a function of gas velocity U_g. The variable σ represents the amplitude of the pressure fluctuations, which are related to the behavior of bubble size [42]. In the four reactors, when U_g was increased to approximately 0.1 m/s, σ increased (above zero), thus indicating that bubbles were gradually being formed, and were passing through the particle bed. **Fig. 6 (b)** shows that further acceleration of the gas led to a consistent increase in the value of σ, thus

demonstrating that the average bubble diameter was increasing. However, when the gas velocity U_g was greater than 0.3 m/s, a small decrease in σ was observed in the case of the rougher reactors (ResinAS, ResinBS and ResinBWS). This could be explained by the fact that roughness can produce a splitting phenomenon within large bubbles or a gas piston. This phenomenon was also predicted by simulations, as reported by Khan et al. [43].

As the particles flow through the bed, the frequency of the bubbles or slugging are characterized by the spectra of their PSDF (**Fig. S1 in SM. 4**) [44]. F_d was derived from the PSDF and corresponds to the maximum value of the power spectral density (PSD), which defines the dominant frequency characterizing the bubbles and slugging [16]. In bubbling fluidization, the PSD has a broad distribution in the frequency range from 0-15 Hz, and is not characterized by a single, identifiable peak corresponding to F_d. In slugging fluidization, the PSD distribution narrows, and has just one peak, corresponding to the value of F_d.

In **Fig. 7**, F_d is expressed as a function of U_g, over the range between 0 and 0.62 m/s fluidizing glass1 particles in the four different MFB reactors with different wall roughness. It was found that F_d is initially close to zero when U_g is approximately 0-0.2 m/s, revealing that there are virtually (almost) no (fixed-bed) bubbles. F_d then gradually increases with increasing U_g, due to the continuously generated bubbles, indicating that the fluidization regimes have transitioned from the fixed bed to bubbling or slugging fluidization. In the case of the Glass, ResinAS, and ResinBS reactors, their PSDF spectra ranged from 0.2-0.47 m/s, with broad distributions, and were not characterized by a single peak corresponding to F_d. This indicates the presence of bubbling fluidization. However, in the case of the ResinBWS reactor, bubbling fluidization ceased at approximately 0.3 m/s. The value of F_d was found to

decrease as a function of increasing U_g, with all reactors. Meanwhile, beyond these velocities, a single peak corresponding to F_d could be identified in the PSDF spectra, revealing the presence of slugging fluidization. Baeyens et al. [45] reported that, for the case of TFBs in general, F_d increases with increasing U_g during bubbling, and becomes independent of U_g during slugging. However, in the present study the value of F_d decreases with increasing U_g during slugging, for all reactors. McDonough et al. [15] and Quan et al. [16] also found a similar trend in MFBs used for the fluidization of Group B particles. This was attributed to the stronger frictional forces induced by smaller values of D_t, which led to the suppression of upward slugging. In addition, **Fig. 7** also shows that during slugging in the ResinAS, ResinBS and ResinBWS reactors (which had rougher walls), F_d was smaller than in the case of the Glass reactor, thus suggesting that an increase in wall roughness could lead to the further suppression of the movement of slugs. This behavior is attributed to the assumption that higher values of wall roughness would increase the time needed for the bubbles or slugs to drift towards to the bed surface and erupt. In other words, the rate of bubble formation and bubble rising velocity are decreased by a higher wall roughness. In another study, it has also been shown that the wall effect is the consequence of the combined effects of a change in geometry (reduced value of D_t) and surface roughness [18].

It is interesting to note that slugging in the ResinBWS reactor started at approximately 0.3 m/s, whereas in the ResinBS reactor it started at approximately 0.47 m/s, suggesting that slugging was advanced in the roughest bed. Thus, at gas velocities greater than 0.3 m/s in the ResinBWS reactor, σ was higher than in the ResinBS reactor. This indicates that the average bubble size occurring in the ResinBWS reactor was greater than in the ResinBS reactor, for $U_g > 0.3$ m/s, thus

suggesting that a strong increase in wall roughness promoted the early appearance of slugging, rather than bubbling. This could be the consequence of delayed bubbles being easier to coalesce with the newly generated bubbles, leading to the formation of larger bubbles (i.e. slugs). We thus infer that only an appropriate increase in wall roughness can effectively suppress slugging, and improve the quality of fluidization.

3.2 Influence of particle size and mechanical vibrations on hydrodynamics in a MFB

Group B (glass1), Group A/C (glass2) and Group C (SiC, Al_2O_3 and TiO_2) particles were fluidized in the ResinBS reactor, in order to study the influence of particle size on the hydrodynamic characteristics of MFBs. A reactor's fluidization properties and hydrodynamic regimes are closely related to the flow characteristics of the fluidized particles. The variation of *HR* (Hausner index), for the five types of fluidized particle was shown in **Tab. 1**. It reveals the presence of free flow (non-cohesive powders) in the case of the glass1 particles, which could be fluidized easily, with no formation of agglomerates. The glass2 and SiC particles were found to have an intermediate level of flowability, which can lead to more difficult fluidization than in the case of glass1 particles. However, the Al_2O_3 and TiO_2 particles exhibited highly cohesive flowability, complicating suspension of the fluidized layer. These results reflect the influence of inter-particulate forces and increased cohesion, as the particle size decreases. In an effort to improve the quality of fluidization, and to promote the fluidization of cohesive particles (Group A/C and C), mechanical vibrations were applied during these trials.

Four levels of vibration intensity (A) (0, 1.37, 2.34 and 3.43) were applied to the ResinBS reactor, in order to investigate the influence of vibration intensity on the fluidization behavior of glass2, SiC, Al_2O_3 and TiO_2 particles. In **Fig. 8**, $\Delta p/(W/A)$ is

plotted as a function of U_g, at the aforementioned levels of vibration intensity. For all particles, in the absence of vibrations, $\Delta p/(W/A)$ increased rapidly with increasing U_g, due to the appearance of the piston and plug phenomena. This initial behavior was systematically followed by the collapse of the piston, and any gas flowing through a preferential passage or channeling resulted in a sharp decline pressure drop Δp. When the gas velocity U_g increased, i.e. high hydrodynamic forces were present, the cohesive structure was gradually dispersed and the agglomerates partially fluidized. Although this partial fluidization resulted in an increase in Δp, it always remained lower than the values of W/A for glass2, SiC and Al_2O_3. In addition, in the case of the latter three types of particles, the partial fluidization zone is highly chaotic and most likely non reproducible. The case of TiO_2 particles is more complex: in **Fig. 8**, it can be seen that the plug phenomenon is following by a pseudo-fluidization regime. This phenomenon is explained in greater detail as follows:

After the application of mechanical vibrations, the plug disappears in the case of glass2 particles. However, the peak values of $\Delta p/(W/A)$ for the SiC and Al_2O_3 particles are understood to decrease with increasing vibrational intensity. Although in the case of SiC, the plug disappeared when the intensity reached Λ=2.34, it was present in the fluidization process of Al_2O_3, until Λ=3.43. This level of vibrational energy is able to disintegrate the cohesive bed particles, i.e. disperse the particles and allow the gas to pass between them or the agglomerates, which is consistent with the conclusions reported by Barletta et al. [23] and Mawatari et al. [25].

In addition, **Fig. 8** shows that the application of mechanical vibrations improves the fluidization of the four types of particles. In the case of glass2, $\Delta p/(W/A)_{ff}$ could be increased to 0.9 at Λ=1.37. However, the fluidization states were unstable when Λ ranged between 0 and 2.34. We consistently found that $\Delta p/(W/A)_{ff}$ would remain

nearly constant, and then decrease with increasing U_g, due to the fact that a greater number of particles could stick to the wall. However, at Λ=3.43 $\Delta p/(W/A)_{ff}$ still remained constant until the end of the fluidization process, thus suggesting that vibrational energy can effectively reduce the adhesion of particles to the wall, thereby improving the continuity and stability of fluidization. In the case of SiC particles, a stable fluidization state could be achieved only for Λ=3.43, with $\Delta p/(W/A)_{ff}$ reaching a nearly constant value of 0.8. With the increasing *HR* (**Tab. 1**), the worse flowability of the particles was observed with the formation of agglomerates due to the increase of the cohesion between the particles. The vibration energy required for fluidization of Al_2O_3 and TiO_2 should be higher than that of SiC (Λ=3.43) consequently. However, **Fig. 8 (c)** shows that the Al_2O_3 particles were fluidized at Λ=1.37, and **Fig. 8 (d)** shows that the TiO_2 particles could be fluidized without the assistance of vibrations (Λ=0). Although the energy required to fluidize mechanically vibrated particles should theoretically increase with increasing *HR*, the tendency appeared inflection point at Al_2O_3 particle. This is due to the fact that the fluidization of Al_2O_3 and TiO_2 particles, which have high cohesive forces, is governed by agglomerates that form spontaneously, and are controlled by a hybrid phenomenon comprising drag forces, vibrational energy and collision energy [19]. However, the fluidized bed behavior of Al_2O_3 and TiO_2 during fluidization is unstable, due to the formation of agglomerates. It is governed by a dynamic process, which is controlled by the constant collision and coalescence of agglomerates, leading to the formation of multistage fluidization regions. Nevertheless, at a vibration intensity Λ=1.37, the value of $\Delta p/(W/A)_{ff}$ for Al_2O_3 increases to 0.8, and for TiO_2 it can be increased to approximately 0.92 when a sufficiently high level of vibration intensity is reached.

The influence of vibration intensity on the minimum fluidizing velocity (U_{mf}) for

these particles was also investigated. The variable $U_{mf\text{-}Wen\text{-}Yu}$ was estimated for all particles using the Wen and Yu [46] formula, which can be written as follows:

$U_{mf\text{-}wen\text{-}Yu} = d_s^2(\rho_s - \rho_g)g/1650\mu_g$ (eq. 5)

where d_s (μm) is the Sauter diameter of the particle, ρ_s (kg/m^3) is the particle density, ρ_g (kg/m^3) is the gas density and μ_g (pa/s) is the gas viscosity.

The experimental value of U_{mf}, referred to here as $U_{mf\Delta P}$, was classically determined by the intersection between the sloping line in the fixed bed and the horizontal line in the fluidized bed. However, this method cannot be applied to the $\Delta p/(W/A)$-U_g curve in the absence of a clear fixed bed region. For this reason, human observation of the video recording was used to determine this point more accurately. It was defined as the minimum fluidization velocity at which all plug phenomena disappeared, and particles started to move, which we refer to here as U_{mfobs}.

In the case of glass2 particles, U_{mf} was determined using U_{mfobs} in the absence of vibrations, and determined from $U_{mf\Delta P}$ under different vibration intensities. In the case of SiC particles, the value of U_{mf} at Γ=3.43 was determined from $U_{mf\Delta P}$. It was found that even when assisted by vibrations, the experimental values of U_{mf} ($U_{mf\Delta P}$ and U_{mfobs}) for both glass2 and SiC were an order of magnitude higher than those computed from $U_{mf\text{-}Wen\text{-}Yu}$. This reveals the influential role of cohesion in the force equilibrium system. However, vibrational energy promotes dispersal (agglomerate fragmentation) of the particles, leading to lower minimum fluidization velocities (**Tab. S2 in SM. 5**) for glass2.

In the case of Al_2O_3 and TiO_2, the values of $U_{mf\text{-}wen\text{-}Yu}$ based on the measured diameter of the particles (**Tab. 1**), and computed from eq. 5, were 5.33×10^{-5}m/s and 1.35×10^{-7}m/s, respectively. However, the fluidized particles (Al_2O_3 and TiO_2) actually

exist in the form of agglomerates, thus leading to a considerable departure from the estimated value of $U_{mf\text{-}wen\text{-}Yu}$. Following the end of fluidization, in all cases we carefully collected the Al_2O_3 and TiO_2 particles from the disengagement portion of the reactor. Then, all the agglomerates were placed on a glass slide and several images were taken with a microscope (Axio Lab. A1 with Axio Cam ICe5) to obtain the representative samples for our analysis. These images were processed with the software "Nano Measure 1.2.5". 200 representative agglomerates were selected for every fluidized case, and their diameters were determined by measuring the maximum linear dimension of the particle (e.g. red line in **Fig. 9**). The work of counting and measurement was done manually with an electronic pen (with enlargement of the images to avoid errors), which allowed us to isolate the surface of the particles and measure the maximum linear dimension. Then the dimensions and the number of agglomerates were processed to build classes of dimensions, and the fraction in number corresponding to each class. Thus, we can plot histograms of the frequency in number (%) as a function of the agglomerate size (maximum linear dimension, μm). The images and size distributions of the Al_2O_3 and TiO_2 particles under different vibration intensities are shown in **Figs. 9** and **10**. From these distributions, the Sauter diameter (referred to as d_{sa}) of the agglomerates was computed from eq. 1, and these are summarized in **Tab. S2 in SM. 5**. In addition, the apparent agglomerate density (referred to as ρ_{aa}) is different to that of single particles, due to the presence of voids. Zhou and Li et al. [47] reported that ρ_{aa} lies in the approximate range from 1.15 ρ_a to 0.85 ρ_t. In the present study, we assumed the value of ρ_{aa} to be ρ_a (aerated density) (1366kg/m^3 and 1535kg/m^3 for Al_2O_3 and TiO_2, respectively). It was shown that the value of $U_{mf\text{-}wen\text{-}Yu}$ based on the properties of agglomerates is 10^3 to 10^6 times greater than that determined from the measured properties of the particles. This reveals that a

higher gas velocity is required for cohesive particles to be fluidized. The error between the value of $U_{mf\text{-}wen\text{-}Yu}$ (based on the properties of particle agglomerates) and U_{mfobs}, $U_{mf\Delta P}$, are plotted for various levels of vibrational intensity in **Figs. 11 (a)** and **(b)**, for Al_2O_3 and TiO_2, respectively. In the case of Al_2O_3, as there is no clear fixed bed region, as shown in **Fig. 8 (c)**, only observed data was used for this comparison. A relatively large error was found between the values of these three groups. This is attributed to the size of the agglomerates in dynamic process, and strongly depends on the ultimate operating gas velocity.

It can be clearly seen that for Al_2O_3 and TiO_2, the influence of vibrational intensity $U_{mf\text{-}wen\text{-}Yu}$ is related to the size of their agglomerates. As shown in **Fig. 12** for the case of Al_2O_3, the agglomerates' size and corresponding value of $U_{mf\text{-}wen\text{-}Yu}$ decreased initially, and then increased with increasing intensity. However, **Fig. 12** shows that in the case TiO_2 the value of $U_{mf\text{-}wen\text{-}Yu}$ decreased with increasing intensity. The presence of two somewhat different trends is related to the cohesion of the particles. Indeed, vibrations can have two different types of influence, in terms of the formation of agglomerates. On the one hand, although this external energy could potentially break up the agglomerates, increasingly strong vibrations could also be expected to improve the probability of particle or agglomerate collisions, thus promoting the growth of particle agglomerates [32].

In addition, the influence of vibrations on the evolution of fluidization regimes for glass2, SiC, Al_2O_3 and TiO_2 were studied by analyzing their PSDF and TF spectra (**SM.6**). In the case of glass2 (**Fig. S2 in SM.6**), the particles were fully fluidized at U_g = 0.04 m/s in the absence of vibrations. A wide range of characteristic frequencies was found in the PSDF, and the pressure fluctuates continuously at these characteristic frequencies, throughout the duration of the TF measurements. This

reveals the presence of bubbling fluidization. Following the application of vibrational energy, the particles progressively became fully fluidized, with a gas velocity U_g = 0.005 m/s. However, there are no characteristic frequency peaks in the PSDF spectra when U_g is increased to 0.030 m/s under Λ ranges from 1.37 to 3.43. This indicates that homogenous fluidization occurred in the initial progress. When U_g was further increased, the characteristic frequency peaks gradually appeared, indicating the onset of bubbling fluidization. It was shown that the application of vibrations triggered the transfer of the plug to homogenous fluidization. In addition, when Λ was increased from 1.37 to 3.43, the range of bubbling fluidization was extended to 0.044 - 0.12 m/s as compared to the initial range: 0.044 - 0.066 m/s. This shows that stronger vibrations could prolong the bubbling fluidization. On the other hand, in the case of the SiC particles (**Fig. S3 in SM.6**) at Λ=3.43, no obvious characteristic frequency peaks were observed when the gas velocity was increased from 0 to 0.04 m/s. This indicates that homogenous fluidization was in progress. The changes in regime induced in glass2 and SiC particles, through the use of vibrations, demonstrate that vibrations can be used to promote a shift in the fluidization patterns of Group A/C and C particles (no agglomerate formation) to that of Group A particles.

In the case of Al_2O_3 and TiO_2 particles, in the presence of vibrations, the behavior of the fluidization regimes is influenced by the agglomerates' properties. In particular, depending on their size and density, the fluidization behavior of both Al_2O_3 and TiO_2 can be altered to that of Group B particles, through the use of vibrations. However, it is shown that the statistical agglomerate size distributions of Al_2O_3 (**Fig. 9**) and TiO_2 (**Fig. 10**) were wide, since under different vibrational intensities they ranged from 0 to 1100 μm, and 800 μm, respectively. For this reason, they are considered to have exhibited the fluidization behavior of mixed particles. In the case of Al_2O_3, most of

the agglomerates belong to Group B particles, and were mixed with a very small quantity of Group A and D particles, under different vibrational intensities. Analysis of the pressure fluctuations, PSDF and TF at U_g of 0.39 m/s, for Γ=1.37 to 3.43, are plotted in **Figs. S4** and **SM.6**. This reveals the presence of bubbling fluidization. However, in the case of the TiO_2 particles, most of the agglomerates were formed by Group A particles, and were mixed with very small quantities of Group B particles at different vibrational intensities. Both with or without the use of vibrations, no bubbles emerged, thus showing that the agglomerate fluidization pattern of TiO_2 particles was more similar to that of Group A particles. Wang et al. [48] first defined a relevant criterion: agglomerate fluidization that primary particle size with nanoscale and bulk density of smaller than 100kg/m^3 meet the agglomerate particulate fluidization (APF) behavior. The main characteristics are the presence of fewer bubbles, uniform agglomerate size distributions. Whereas the agglomerate fluidization that primary size with nano-, micro- or sub-micro scale and bulk density of higher than 1000kg/m^3 meet the agglomerate bubbling fluidization (ABF) behavior. The main characteristics are the presence of bubbles and broad agglomerate size distributions. In the present study, Al_2O_3 was definitely close to the criterion for ABF behavior, whereas TiO_2 was partially accord with APF behavior. However, the TiO_2 particles were unable to reach their bulk density characteristics, which could be due to limitations in the types of particles used for the study.

4. Conclusions

In the present study, 4 mm Micro-fluidized beds (MFBs) with different values of wall roughness were tested. They were manufactured using different materials and methods: glass, and resin (constructed by stereo-lithographic 3D printing (3D-PR) technique). Firstly, the influence of wall roughness on MFB hydrodynamics was

investigated for the fluidization of Group B particles. In addition, the influence of particle size and mechanical vibrations on the hydrodynamics of MFB was analyzed, by comparing the fluidization behavior of Group A/C (glass2) and Group C (SiC, Al_2O_3 and TiO_2) particles.

-When the particles are fully fluidized, $\Delta p/(W/A)$ increases with increasing wall roughness, and above than unity due to the increased wall friction component of the force equilibrium system. An increase in wall friction is also one of the significant contributors to the wall effect. An appropriate increase in wall roughness can contribute to the suppression of the slugging phenomenon.

-The flowability of particles decreases with decreasing particle size, due to their greater cohesive forces, which makes it more difficult to fluidize them. Mechanical vibrations alleviated or destroyed the plug phenomenon, and improved the quality of particle fluidization. However, the vibrational energy needed to fully fluidize the particles did not appear to increase with cohesion force. On the contrary, in the case of the Al_2O_3 particles, an inflection point was observed due to the formation of agglomerates.

-Mechanical vibrations promoted a shift of the fluidization regimes of Group A/C or C particles (no agglomerate formation) to that of Group A particles. It also promoted a shift of the fluidization regimes of Group C particles (with agglomerate formation) to that of mixed particles. In addition, vibrations can not only break up the agglomerates, but also improve the probability of contact between particles, which favors the growth of agglomerates.

Overall, the successful fluidization of Group A/C and C particles indicates the potential for particle mixing, coating, and catalytic reactions in MFB reactors. In particular, miniaturized fluidized bed offers the potential for a reduction in the

duration and cost of raw materials, thus making it more cost effective to produce high-value chemical products.

Nomenclature

ABF	Agglomerate bubbling fluidization	
APF	Agglomerate particulate fluidization	
A_v	Vibration amplitudes	mm
TFBs	Traditional fluidized beds	
C_u	The index of size distribution	
d_i	The average dimension of the particle in this class *i*	
d_{i60}	Particle diameter with the cumulative percentage of 60%	
d_{i10}	Particle diameter with the cumulative percentage of 10%	
d_s	Sauter diameter	μm
d_{sa}	Sauter diameter of the agglomerates	μm
D_t	Bed diameter	mm
D_t/d_s	Bed-to-particle diameter ratio	
FFT	Fast Fourier transform	
F_d	Dominant frequency	
f_s	Optimum sampling frequency	
f_v	Vibration frequency	Hz
HR	Hausner index	
H_s	Static bed height	mm
MFBs	Micro-fluidized beds	
N	Sample number	
N_i	The number of particles in class *i*	
PFs	Pressure fluctuations	Pa
PSDF	Power spectral density function	
PSD	Power spectral density	
R_a	Arithmetic mean height of the roughness profiles	μm
SM	Supplementary materials	
TF	Time– frequency	
U_g	Gas velocity	m/s
U_{mf}	Minimum fluidization velocity	m/s
U_{mfobs}	Minimum fluidization velocity determined by observation	m/s
$U_{mf\text{-}Wen\text{-}Yu}$	Minimum fluidization velocity calculated by Wen and Yu equation	m/s
$U_{mf\Delta P}$	Minimum fluidization velocity determined by pressure to gas velocity figure	m/s
W/A	Particles bed weight per cross-sectional area	Pa
Δp	Pressure drop	Pa
$\Delta p/(W/A)$	Normalized pressure drop	
$\Delta p/(W/A)_{ff}$	$\Delta p/(W/A)$ when the particles were fully fluidized	
ρ_a	Aerated density	kg/m^3
ρ_{aa}	Apparent density of agglomerates	kg/m^3
ρ_g	Gas density	kg/m^3
ρ_s	Particle density	kg/m^3
ρ_t	Tapped density	kg/m^3
μ_g	Gas viscosity	Pa/s
Λ	Vibration intensity	
$\bar{x}$	Mean value	Pa
σ	Standard deviation	Pa
3D-PR	3D printing	

Declaration of Competing Interest

The authors declare that they have no known competing financial interests or personal relationships that could have appeared to influence the work reported in this paper.

Acknowledgments

Zhuojun Jiang would like to thank China Scholarship Council for his PhD stipend.

References

[1] B. Potic, S. R. A. Kersten, M. Ye, M. A. van der Hoef, J. A. M. Kuipers, W. P. M. van Swaaij. Fluidization with hot compressed water in micro-reactors. Chemical Engineering Science, 60 (22), (2005) 5982-5990. https://doi.org/10.1016/j.ces.2005.04.047

[2] Fang Wang, Xi Zeng, Yonggang Wang, Jian Yu, Guangwen Xu. Characterization of coal char gasification with steam in a micro-fluidized bed reaction analyzer. Fuel Processing Technology, 141 (2016) 2-8. https://doi.org/10.1016/j.fuproc.2015.04.025

[3] Ye Li, Hui Wang, Weicheng Li, Zhenshan Li, Ningsheng Cai. CO_2 Gasification of a Lignite Char in Microfluidized Bed Thermogravimetric Analysis for Chemical Looping Combustion and Chemical Looping with Oxygen Uncoupling. Energy & Fuels, 33 (1), (2019) 449-459. https://doi.org/10.1021/acs.energyfuels.8b02909

[4] Ye Shen, Xian Li, Zhiyi Yao, Xiaoqiang Cui, Chi-Hwa Wang. CO_2 gasification of woody biomass: Experimental study from a lab-scale reactor to a small-scale autothermal gasifier. Energy, 170 (2019) 497-506. https://doi.org/10.1016/j.energy.2018.12.176

[5] Yuming Zhang, Mengxuan Zhao, Rongxuan Linghu, Chengxiu Wang, Shu Zhang. Comparative kinetics of coal and oil shale pyrolysis in a micro fluidized bed reaction analyzer. Carbon Resources Conversion, 2 (3), (2019) 217-224. https://doi.org/10.1016/j.crcon.2019.10.001

[6] Ye Li, Zhenshan Li, Hui Wang, Ningsheng Cai. CaO carbonation kinetics determined using micro-fluidized bed thermogravimetric analysis. Fuel, 264

(2020) 116823. https://doi.org/10.1016/j.fuel.2019.116823

[7] Xi Zeng, Jianling Zhang, Mohammed Haruna Adamu, Fang Wang, Zhennan Han, Qingxin Zheng, Lijuan Zhang, Guangwen Xu. Behavior and Kinetics of Drying, Pyrolysis, Gasification, and Combustion Tested by a Microfluidized Bed Reaction Analyzer for the Staged-Gasification Process. Energy & Fuels, 34 (2), (2020) 2553-2565. https://doi.org/10.1021/acs.energyfuels.9b03707

[8] Zhennan Han, Junrong Yue, Sulong Geng, Dandan Hu, Xuejing Liu, Sabo Bello Suleiman, Yanbin Cui, Dingrong Bai, Guangwen Xu. State-of-the-art hydrodynamics of gas-solid micro fluidized beds. Chemical Engineering Science, 232 (2021) 116345. https://doi.org/10.1016/j.ces.2020.116345

[9] Xinhua Liu, Guangwen Xu, Shiqiu Gao. Micro fluidized beds: Wall effect and operability. Chemical Engineering Journal, 137 (2), (2008) 302-307. https://doi.org/10.1016/j.cej.2007.04.035

[10] Q. j Guo, Y. Xu, X. Yue. Fluidization Characteristics in Micro-Fluidized Beds of Various Inner Diameters. Chemical Engineering & Technology, 32 (12), (2009) 1992-1999. https://doi.org/10.1002/ceat.200900092

[11] Akhil Rao, Jennifer S. Curtis, Bruno C. Hancock, Carl Wassgren. The effect of column diameter and bed height on minimum fluidization velocity. AIChE Journal, 56 (9), (2010) 2304-2311. https://doi.org/10.1002/aic.12161

[12] Fei Wang, Liang-Shih Fan. Gas−Solid Fluidization in Mini- and Micro-channels. Industrial & Engineering Chemistry Research, 50 (8), (2011) 4741-4751. https://doi.org/10.1021/ie102245m

[13] F. Vanni, B. Caussat, C. Ablitzer, M. Brothier. Effects of reducing the reactor diameter on the fluidization of a very dense powder. Powder Technology, 277 (2015) 268-274. https://doi.org/10.1016/j.powtec.2015.03.010

[14] Vikrant Verma, Johan T. Padding, Niels G. Deen, J. A. M. Kuipers. Effect of bed size on hydrodynamics in 3-D gas–solid fluidized beds. AIChE Journal, 61 (5), (2015) 1492-1506. https://doi.org/10.1002/aic.14738

[15] J. R. McDonough, R. Law, D. A. Reay, V. Zivkovic. Fluidization in small-scale gas-solid 3D-printed fluidized beds. Chemical Engineering Science, 200 (2019) 294-309. https://doi.org/10.1016/j.ces.2019.01.048

[16] Haiqin Quan, Nouria Fatah, Chundong Hu. Diagnosis of hydrodynamic regimes from large to micro-fluidized beds. Chemical Engineering Journal, 391 (2020) 123615. https://doi.org/10.1016/j.cej.2019.123615

[17] Jie Xiang, Yanguo Zhang, Qinghai Li. Effect of bed size on the gas–solid flow characterized by pressure fluctuations in bubbling fluidized beds. Particuology, 47 (2019) 1-9. https://doi.org/10.1016/j.partic.2018.11.004

[18] Yupeng Xu, Tingwen Li, Jordan Musser, Xiaoxing Liu, Guangwen Xu, William A. Rogers. CFD-DEM modeling the effect of column size and bed height on minimum fluidization velocity in micro fluidized beds with Geldart B particles. Powder Technology, 318 (2017) 321-328. https://doi.org/10.1016/j.powtec.2017.06.020

[19] Federica Raganati, Riccardo Chirone, Paola Ammendola. Gas–solid fluidization of cohesive powders. Chemical Engineering Research and Design, 133 (2018) 347-387. https://doi.org/10.1016/j.cherd.2018.03.034

[20] Mengqi Han, Yandaizi Zhou, Jesse Zhu. Improvement on flowability and fluidization of Group C particles after nanoparticle modification. Powder Technology, 365 (2020) 208-214. https://doi.org/10.1016/j.powtec.2019.07.026

[21] Xiaolin Zhu, Qiang Zhang, Cang Huang, Yao Wang, Chaohe Yang, Fei Wei. Validation of surface coating with nanoparticles to improve the flowability of fine cohesive powders. Particuology, 30 (2017) 53-61. https://doi.org/10.1016/j.partic.2016.09.001

[22] Samir Salameh, Jesús Gómez-Hernández, Aristeidis Goulas, Hao Van Bui, J. Ruud van Ommen. Advances in scalable gas-phase manufacturing and processing of nanostructured solids: A review. Particuology, 30 (2017) 15-39. https://doi.org/10.1016/j.partic.2016.07.003

[23] Diego Barletta, Massimo Poletto. Aggregation phenomena in fluidization of cohesive powders assisted by mechanical vibrations. Powder Technology, 225 (2012) 93-100. https://doi.org/10.1016/j.powtec.2012.03.038

[24] Yoshihide Mawatari, Tetsu Koide, Yuji Tatemoto, Shigeo Uchida, Katsuji Noda. Effect of particle diameter on fluidization under vibration. Powder Technology, 123 (1), (2002) 69-74. https://doi.org/10.1016/S0032-5910(01)00432-6

[25] Yoshihide Mawatari, Yasumasa Hamada, Masato Yamamura, Hiroyuki Kage. Flow Pattern Transition of Fine Cohesive Powders in a Gas-Solid Fluidized Bed under Mechanical Vibrating Conditions. Procedia Engineering, 102 (2015) 945-951. https://doi.org/10.1016/j.proeng.2015.01.216

[26] Jingsi Yang, Tao Zhou, Lianying Song. Agglomerating vibro-fluidization behavior of nano-particles. Advanced Powder Technology, 20 (2), (2009) 158-163.

https://doi.org/10.1016/j.apt.2008.06.002

[27] Federica Raganati, Paola Ammendola, Riccardo Chirone. Role of Acoustic Fields in Promoting the Gas-Solid Contact in a Fluidized Bed of Fine Particles. KONA Powder and Particle Journal, 32 (2015) 23-40. https://doi.org/10.14356/kona.2015006

[28] Chao Zhu, Guangliang Liu, Qun Yu, Robert Pfeffer, Rajesh N. Dave, Caroline H. Nam. Sound assisted fluidization of nanoparticle agglomerates. Powder Technology, 141 (1), (2004) 119-123. https://doi.org/10.1016/j.powtec.2004.01.023

[29] M. A. S. Quintanilla, J. M. Valverde, A. Castellanos, D. Lepek, R. Pfeffer, R. N. Dave. Nanofluidization as affected by vibration and electrostatic fields. Chemical Engineering Science, 63 (22), (2008) 5559-5569. https://doi.org/10.1016/j.ces.2008.08.012

[30] Lianying Song, Tao Zhou, Jingsi Yang. Fluidization behavior of nano-particles by adding coarse particles. Advanced Powder Technology, 20 (4), (2009) 366-370. https://doi.org/10.1016/j.apt.2009.02.010

[31] Wei Zhang, Ming Zhao. Fluidisation behaviour of silica nanoparticles under horizontal vibration. Journal of Experimental Nanoscience, 5 (1), (2010) 69-82. https://doi.org/10.1080/17458080903260944

[32] Chunbao Xu, Jesse Zhu. Parametric study of fine particle fluidization under mechanical vibration. Powder Technology, 161 (2), (2006) 135-144. https://doi.org/10.1016/j.powtec.2005.10.002

[33] E. Marring, A. C. Hoffmann, L. P. B. M. Janssen. The effect of vibration on the fluidization behaviour of some cohesive powders. Powder Technology, 79 (1), (1994) 1-10. https://doi.org/10.1016/0032-5910(94)02810-9

[34] Jeffrey R. Wank, Steven M. George, Alan W. Weimer. Vibro-fluidization of fine boron nitride powder at low pressure. Powder Technology, 121 (2), (2001) 195-204. https://doi.org/10.1016/S0032-5910(01)00337-0

[35] Chunbao Xu, Jesse Zhu. Experimental and theoretical study on the agglomeration arising from fluidization of cohesive particles—effects of mechanical vibration. Chemical Engineering Science, 60 (23), (2005) 6529-6541. https://doi.org/10.1016/j.ces.2005.05.062

[36] N. Fatah. Study and comparison of micronic and nanometric powders: Analysis of physical, flow and interparticle properties of powders. Powder Technology, 190

(2009) 41-47. https://doi.org/10.1016/j.powtec.2008.04.055

[37] F. Schlosser, Eléments de mécanique des sols, Presses de l'Ecole Nationale des Ponts et Chaussées, Paris, 1988.

[38] Nouria Fatah, Djamel Turki. Fluidization and study of nanometric powders behavior: Numerical approach to estimate the agglomerates sizes. Particle Technology, AIChE5 (2006) 16.

[39] Or-ampai Jaiboon, Benjapon Chalermsinsuwan, Lursuang Mekasut, Pornpote Piumsomboon. Effect of flow pattern on power spectral density of pressure fluctuation in various fluidization regimes. Powder Technology, 233 (2013) 215-226. https://doi.org/10.1016/j.powtec.2012.09.014

[40] Leon Cohen, Time-frequency analysis / Leon Cohen, Prentice Hall PTR, Englewood Cliffs, N.J, (1995).

[41] R. Wilson, D. Dini, B. Van Wachem. The influence of surface roughness and adhesion on particle rolling. Powder Technology, 312 (2017) 321-333. https://doi.org/10.1016/j.powtec.2017.01.080

[42] Jie Xiang, Qinghai Li, Zhongchao Tan, Yanguo Zhang. Characterization of the flow in a gas-solid bubbling fluidized bed by pressure fluctuation. Chemical Engineering Science, 174 (2017) 93-103. https://doi.org/10.1016/j.ces.2017.09.001

[43] Mohammed N. Khan, Tariq Shamim. Influence of Specularity Coefficient on the Hydrodynamics and Bubble Statistics of an Annular Fluidized Bed Reactor. Energy Procedia, 105 (2017) 1998-2003. https://doi.org/10.1016/j.egypro.2017.03.573

[44] F. Johnsson, R. C. Zijerveld, J. C. Schouten, C. M. van den Bleek, B. Leckner. Characterization of fluidization regimes by time-series analysis of pressure fluctuations. International Journal of Multiphase Flow, 26 (4), (2000) 663-715. https://doi.org/10.1016/S0301-9322(99)00028-2

[45] J. Baeyens, D Geldart. An investigation into slugging fluidized beds. Chemical Engineering Science, 29 (1), (1974) 255-265. https://doi.org/10.1016/0009-2509(74)85051-7

[46] C. Y. Wen, Y. H. Yu. A generalized method for predicting the minimum fluidization velocity. AIChE Journal, 12 (3), (1966) 610-612. https://doi.org/10.1002/aic.690120343

[47] Tao Zhou, Hongzhong Li. Estimation of agglomerate size for cohesive particles

during fluidization. Powder Technology, 101 (1), (1999) 57-62. https://doi.org/10.1016/S0032-5910(98)00148-X

[48] Wang Yao, Gu Guangsheng, Wei Fei, Wu Jun. Fluidization and agglomerate structure of SiO_2 nanoparticles. Powder Technology, 124 (1), (2002) 152-159. https://doi.org/10.1016/S0032-5910(01)00491-0

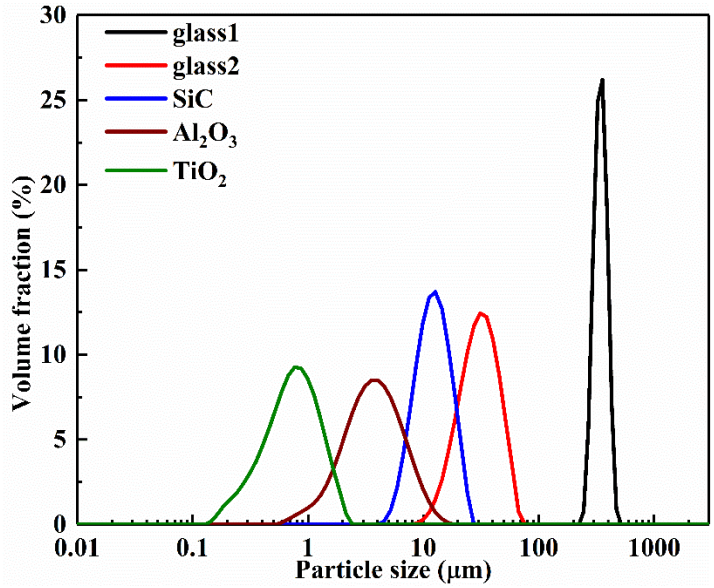

Fig. 1. Size distributions of the five sets of particles (glass1, glass2, SiC, Al_2O_3 and TiO_2).

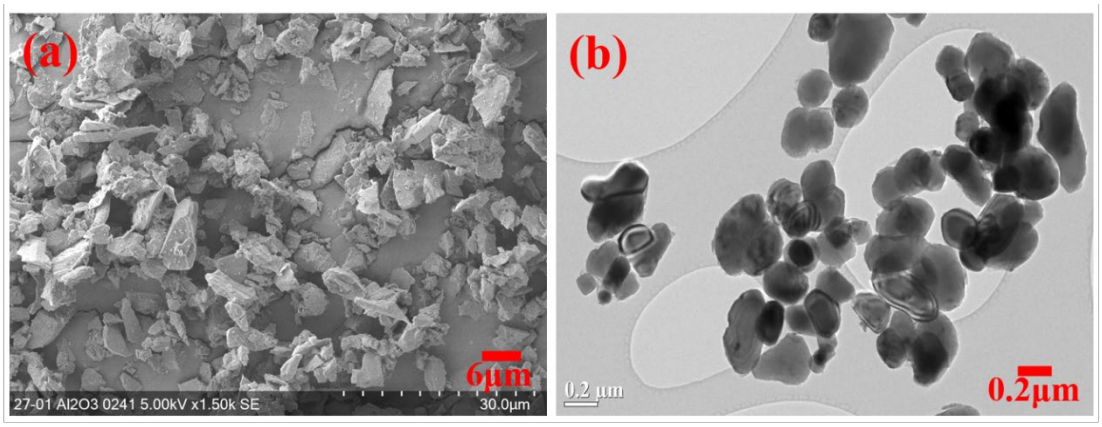

Fig. 2. SEM image of primary Al_2O_3 (a), and TEM image of primary TiO_2 (b).

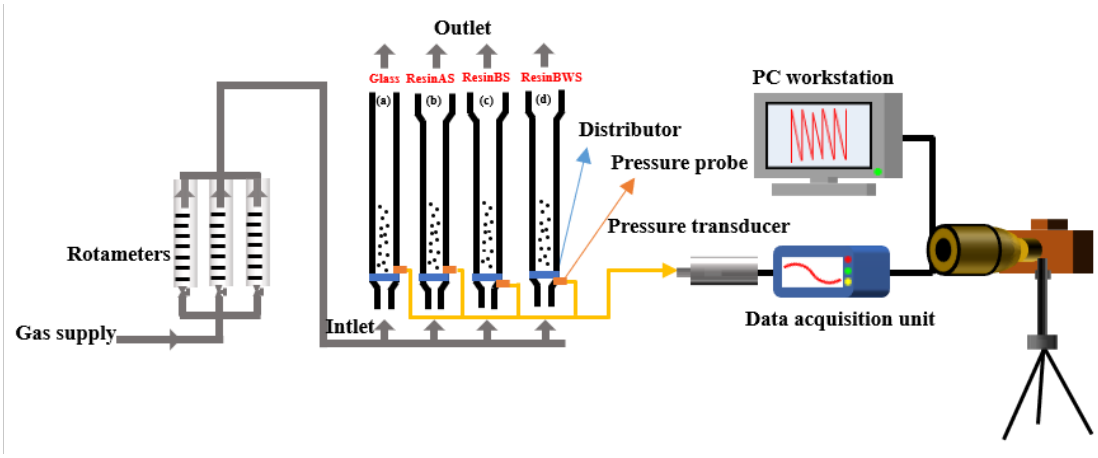

Fig. 3. Schematic view of the experimental set-up. (a) fluidized bed made of glass, (b), (c) and (d) fluidized beds built using 3D-PR.

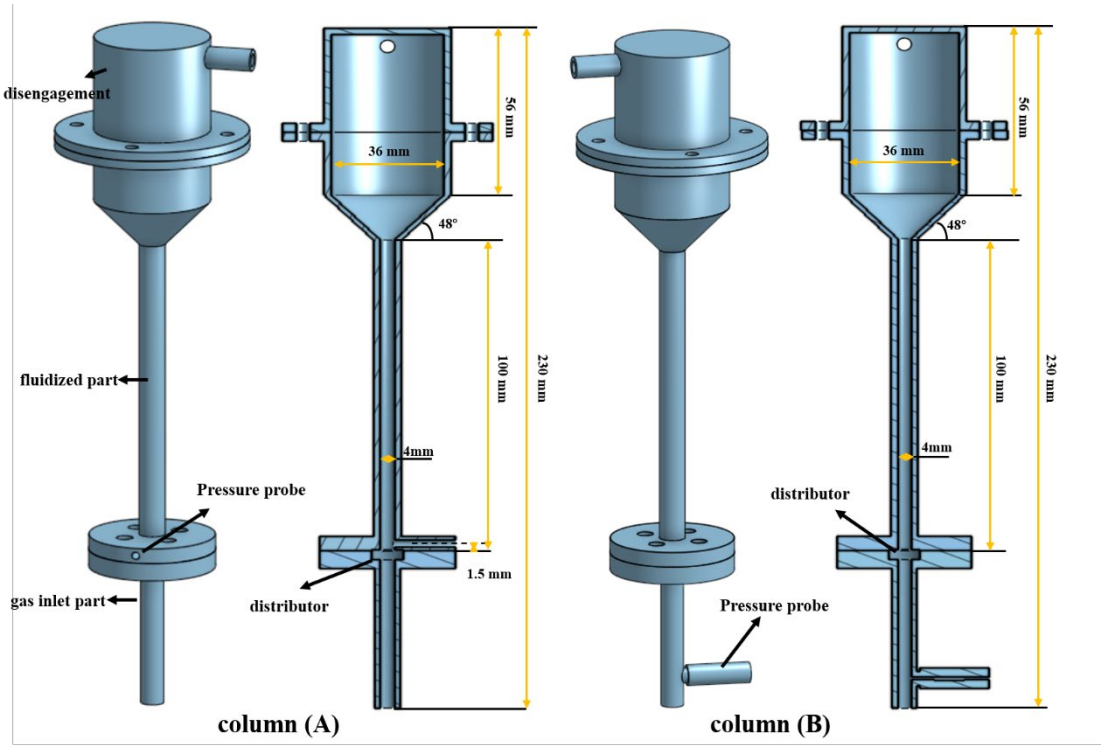

Fig. 4. Two MFB models produced using 3D-PR: column (A) and (B), with their corresponding cross- sectional views.

Fig. 5. Mechanical vibration-assisted MFB fluidization setup.

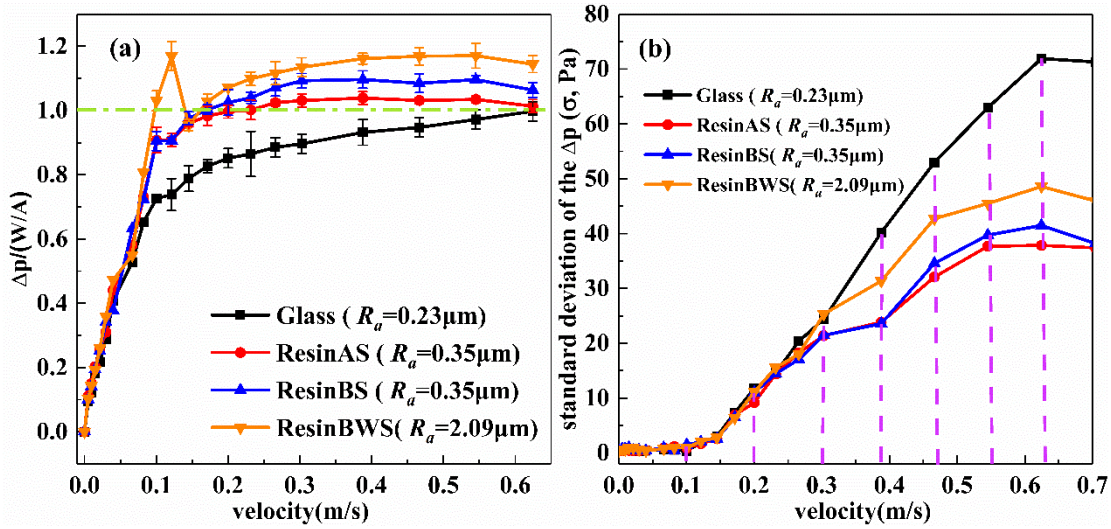

Fig. 6. Normalized pressure drop $\Delta p/(W/A)$ and its standard deviation as a function of the gas velocity required to fluidize glass1 particles in 4 different MFB reactors (Glass, ResinAS, ResinBS, and ResinBWS) having different values of wall roughness (R_a).

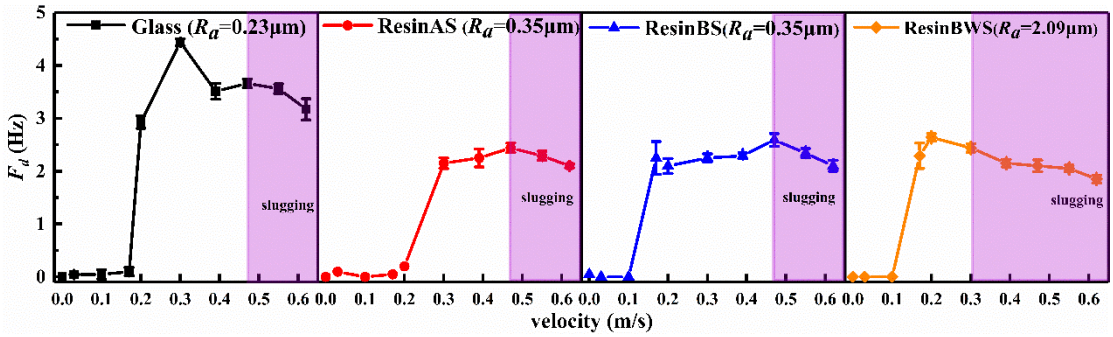

Fig. 7. Variation of F_d as a function of gas velocity, over the range between 0 m/s and 0.62 m/s, for the fluidization of glass1 particles in four different MFB reactors (Glass, ResinAS, ResinBS, and ResinBWS), having different values of wall roughness.

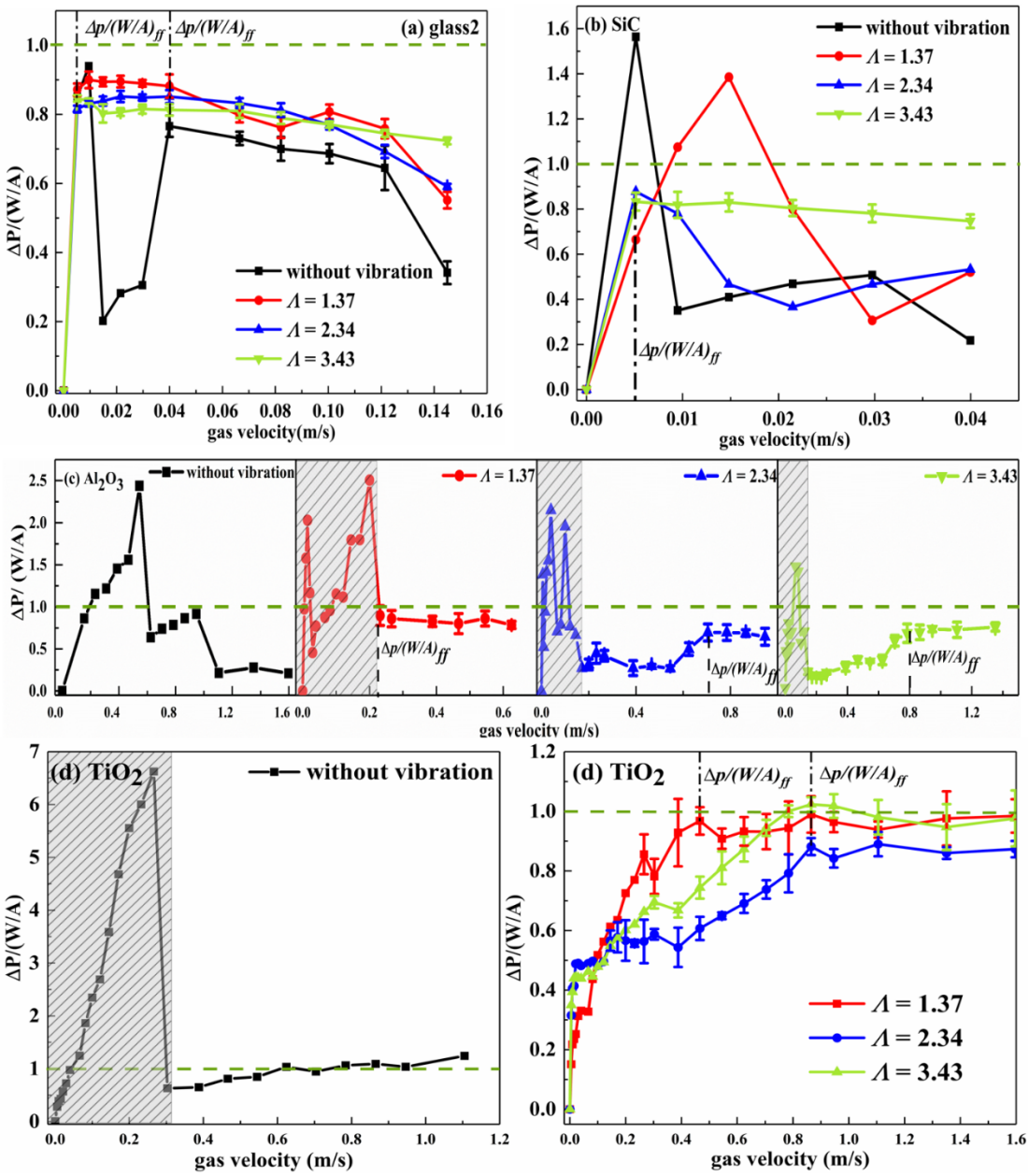

Fig. 8. $\Delta p/(W/A)$ plotted as a function of gas velocity for the fluidization of glass2 (a), SiC (b), Al_2O_3 (c), and TiO_2 (d) with a ResinBS bed, at four levels of mechanical vibration intensity.

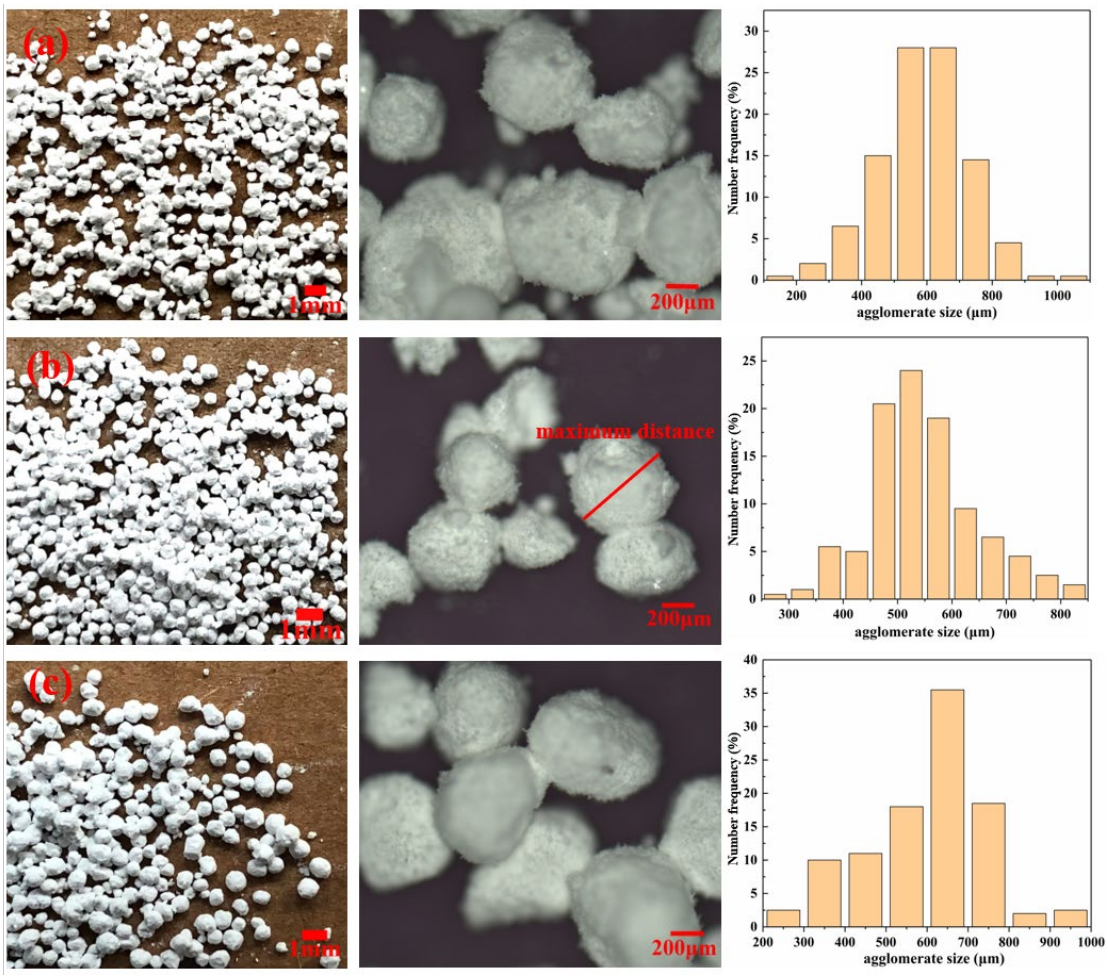

Fig. 9. Images and size distributions for the Al_2O_3 agglomerates under different vibrational intensities: (a) A=1.37, (b) A=2.34 and (c) A=3.43.

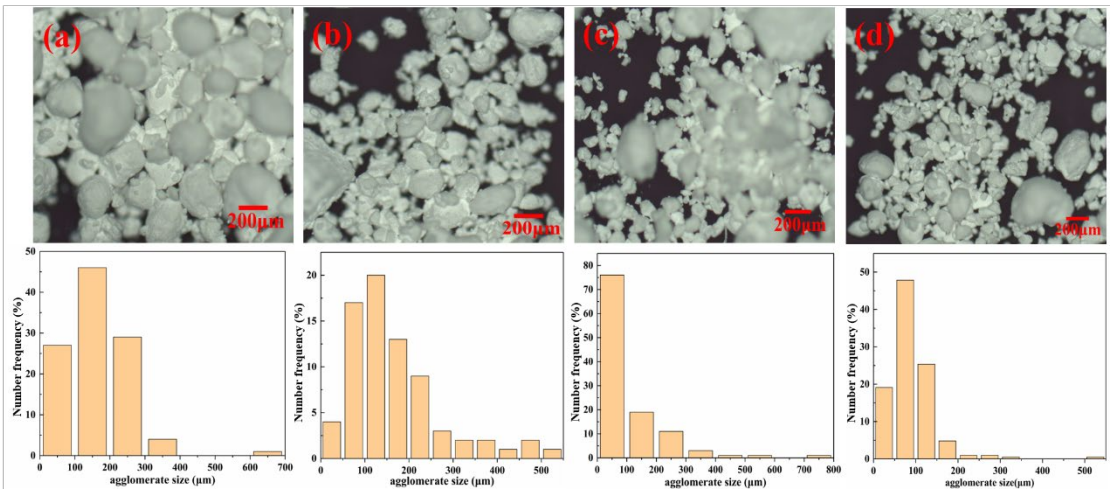

Fig. 10. Images and size distributions for the TiO_2 agglomerates under different vibrational intensities: (a) without vibrations, (b) A=1.37, (c) A=2.34 and (d) A=3.43.

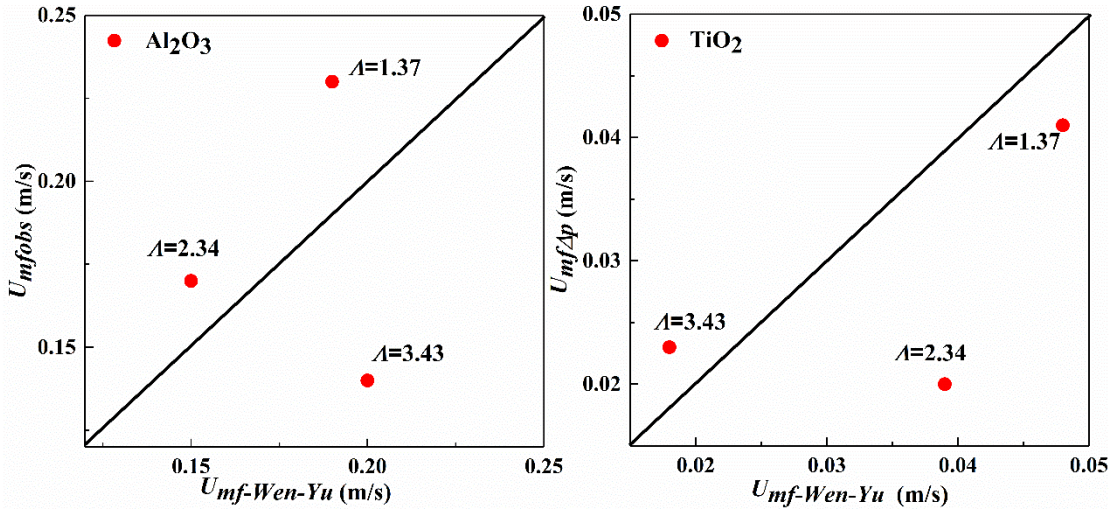

Fig. 11. Predicted minimum fluidization velocity errors at 3 different values of vibrational intensity: Λ=1.37, 2.34 and 3.43, for Al_2O_3 (a), and TiO_2 (b).

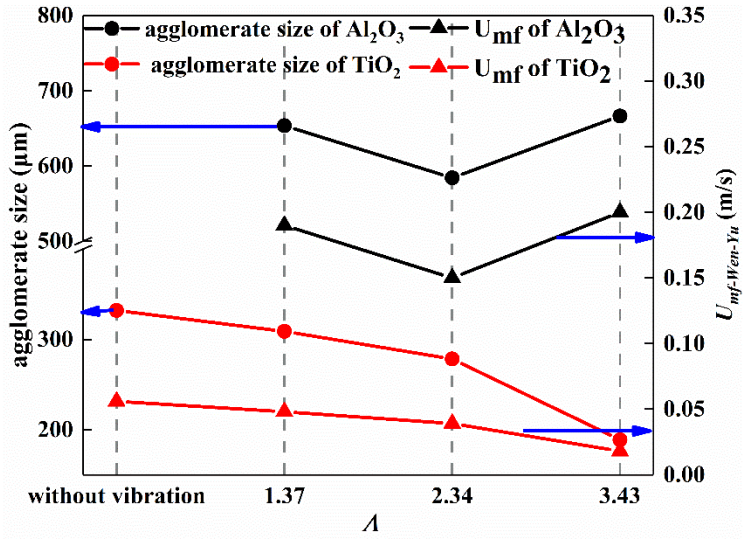

Fig. 12. Agglomerate size (left axis) and $U_{mf\text{-}wen\text{-}Yu}$ (right axis) as a function of increasing vibrational intensity, for Al_2O_3 and TiO_2 particles.

Tab. 1. Physical properties of the particles.

Particles	Particle diameter (d_s, $\times 10^{-6}$m)	Density (ρ_s, kg/m^3)	Uniformity (C_u)	Geldart Group	Hausner Index (HR)	Flowability
glass1	347	2479±3.7	1.23	B	1.04	free flow
glass2	29.6	2488±4.5	1.62	A/C	1.21	intermediate-free flow
SiC	12	3201±11.8	1.74	C	1.30	intermediate-free flow
Al_2O_3	3.22	3963±10.0	2.09	C	1.63	non-free flow
TiO_2	0.64	4104±13.5	2.53	C	1.82	non-free flow

Tab. 2. Details of all MFBs used in this study.

Name	Bed Materials	Pressure Probe position	Treatment applied to the inner wall	R_a (μm)
Glass	glass	1.5mm above distributor	/	0.23
ResinAS	resin	1.5mm above distributor	Surface polishing / smoothing	0.35
ResinBS	resin	below distributor	Surface polishing / smoothing	0.35
ResinBWS	resin	below distributor	Without surface polishing / smoothing	2.09

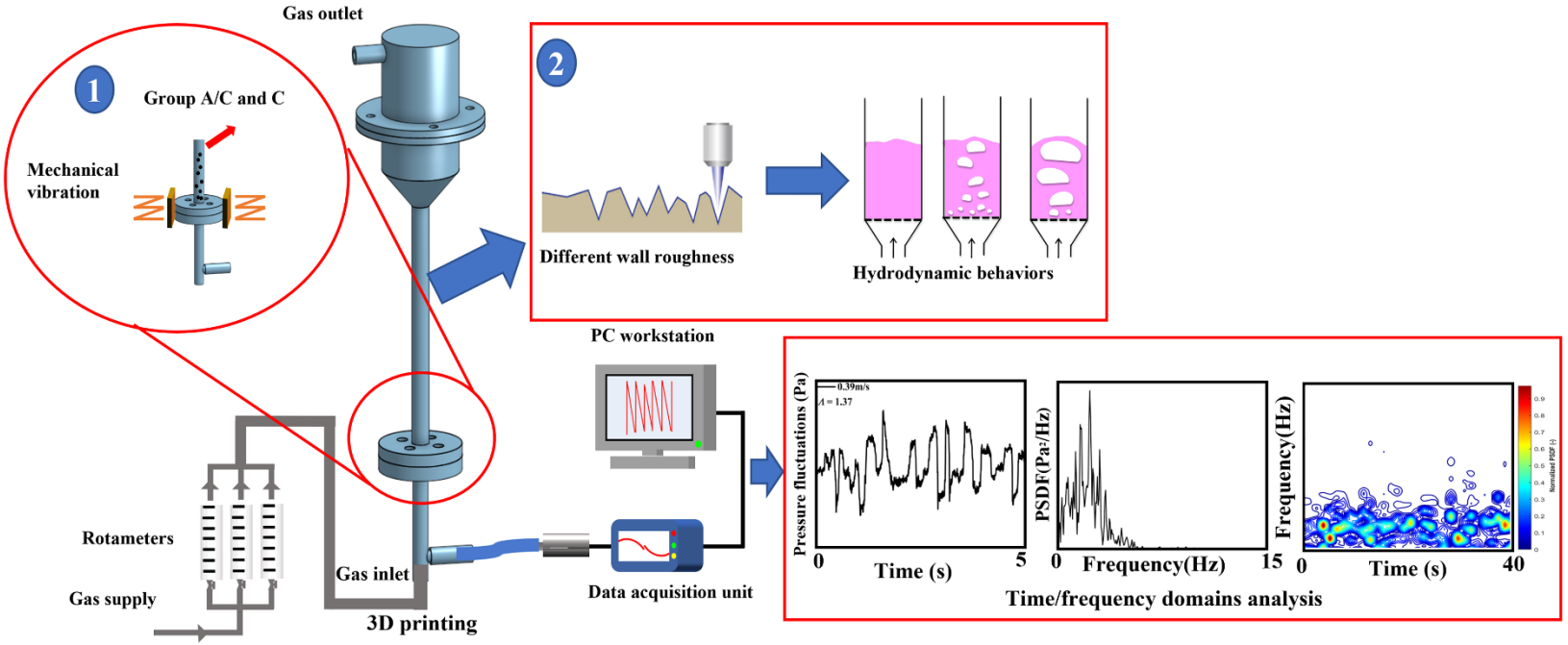
Gas outlet
1
Group A/C and C
Mechanical vibration
2
Different wall roughness
Hydrodynamic behaviors
PC workstation
Rotameters
Gas supply
Gas inlet
3D printing
Data acquisition unit
Pressure fluctuations (Pa)
0.39m/s
A = 1.37
0
Time (s)
5
PSDF(Pa²/Hz)
0
Frequency(Hz)
15
Frequency(Hz)
0
Time (s)
40
Time/frequency domains analysis